



A single-crystal neutron diffraction study of wardite, $\text{NaAl}_3(\text{PO}_4)_2(\text{OH})_4 \cdot 2\text{H}_2\text{O}$

G. Diego Gatta^{1,2} · Alessandro Guastoni³ · Oscar Fabelo⁴ · Maria Teresa Fernandez-Diaz⁴

Received: 29 September 2018 / Accepted: 8 November 2018 / Published online: 19 November 2018
© Springer-Verlag GmbH Germany, part of Springer Nature 2018

Abstract

The crystal structure and crystal chemistry of wardite, ideally $\text{NaAl}_3(\text{PO}_4)_2(\text{OH})_4 \cdot 2\text{H}_2\text{O}$, was investigated by single-crystal neutron diffraction (data collected at 20 K) and electron microprobe analysis in wavelength-dispersive mode. The empirical formula of the sample used in this study is: $(\text{Na}_{0.91}\text{Ca}_{0.01})_{\Sigma=0.92}(\text{Al}_{2.97}\text{Fe}^{3+}_{0.05}\text{Ti}_{0.01})_{\Sigma=3.03}(\text{P}_{2.10}\text{O}_8)(\text{OH})_4 \cdot 1.74\text{H}_2\text{O}$. The neutron diffraction data confirm that the crystal structure of wardite can be described with a tetragonal symmetry (space group $P4_12_12$, $a=b=7.0577(5)$ and $c=19.0559(5)$ Å at 20 K) and consists of sheets made of edge-sharing Na-polyhedra and Al-octahedra along with vertex-sharing Al-octahedra, parallel to (001), connected by P-tetrahedra and H bonds to form a (001) layer-type structure, which well explains the pronounced {001} cleavage of the wardite crystals. The present data show that four crystallographically independent H sites occur in the structure of wardite, two belonging to a H_2O molecule (i.e., H1–O6–H2) and two forming hydroxyl groups (i.e., O5–H3 and O7–H4). The location of the hydrogen atoms allows us to define the extensive network of H bonds: the H atoms belonging to the H_2O molecule form strong H bonds, whereas both the H atoms belonging to the two independent hydroxyl groups form weak interactions with bifurcated bonding schemes. As shown by the root-mean-square components of the displacement ellipsoids, oxygen and hydrogen atoms have slightly larger anisotropic displacement parameters compared to the other sites (populated by P, Al and Na). The maximum ratio of the *max* and *min* root-mean-square components of the displacement ellipsoids is observed for the protons of the hydroxyl groups, which experience bifurcated H-bonding schemes. A comparative analysis of the crystal structure of wardite and fluorowardite is also provided.

Keywords Wardite · Phosphates · Single-crystal neutron diffraction · Crystal chemistry · Hydrogen bonding

Introduction

Wardite, ideally $\text{NaAl}_3(\text{PO}_4)_2(\text{OH})_4 \cdot 2\text{H}_2\text{O}$, is a hydrous phosphate mineral discovered and described by Davison (1896). It was found in cavities in variscite nodules from the Clay Canyon deposit (near Fairfield) in Utah County (Davison 1896; Kampf et al. 2014). Wardite is

a hydrothermal mineral, which occurs in phosphate-rich zones of granite pegmatites. After a series of experiments aimed at describing the chemical nature and the symmetry of the wardite crystals (e.g., Hurlbut 1952; Heritsch 1955), its structure was solved by Fanfani et al. (1970), on the basis of single-crystal X-ray intensity data (collected by Weissenberg method with multiple-film integrated photographs) and using a crystal from the type locality. The authors described the structure of wardite in the space group $P4_12_12$, with unit-cell constants $a=b \sim 7.03$ Å, $c \sim 19.04$ Å (and $\alpha=\beta=\gamma=90^\circ$). The wardite structure consists of sheets of Al- and Na-coordination polyhedra sharing vertices and edges. These sheets, parallel to (001), are connected to each other along the [001] direction by PO_4 -tetrahedra (and H bonds) (Fig. 1). The structure model reported by Fanfani et al. (1970) is consistent, in terms of bond distances and angles of the Na-, Al- and P-polyhedra. However, the quality of the data at that time did not allow

✉ G. Diego Gatta
diego.gatta@unimi.it

¹ Dipartimento di Scienze della Terra, Università degli Studi di Milano, Via Botticelli 23, 20133 Milan, Italy

² CNR-Istituto di Cristallografia, Via Amendola 122/O, 70126 Bari, Italy

³ Dipartimento di Geoscienze, Università degli Studi di Padova, Via G. Gradenigo 6, 35131 Padua, Italy

⁴ Institut Laue-Langevin, 71 Avenue des Martyrs, 38042 Grenoble, France

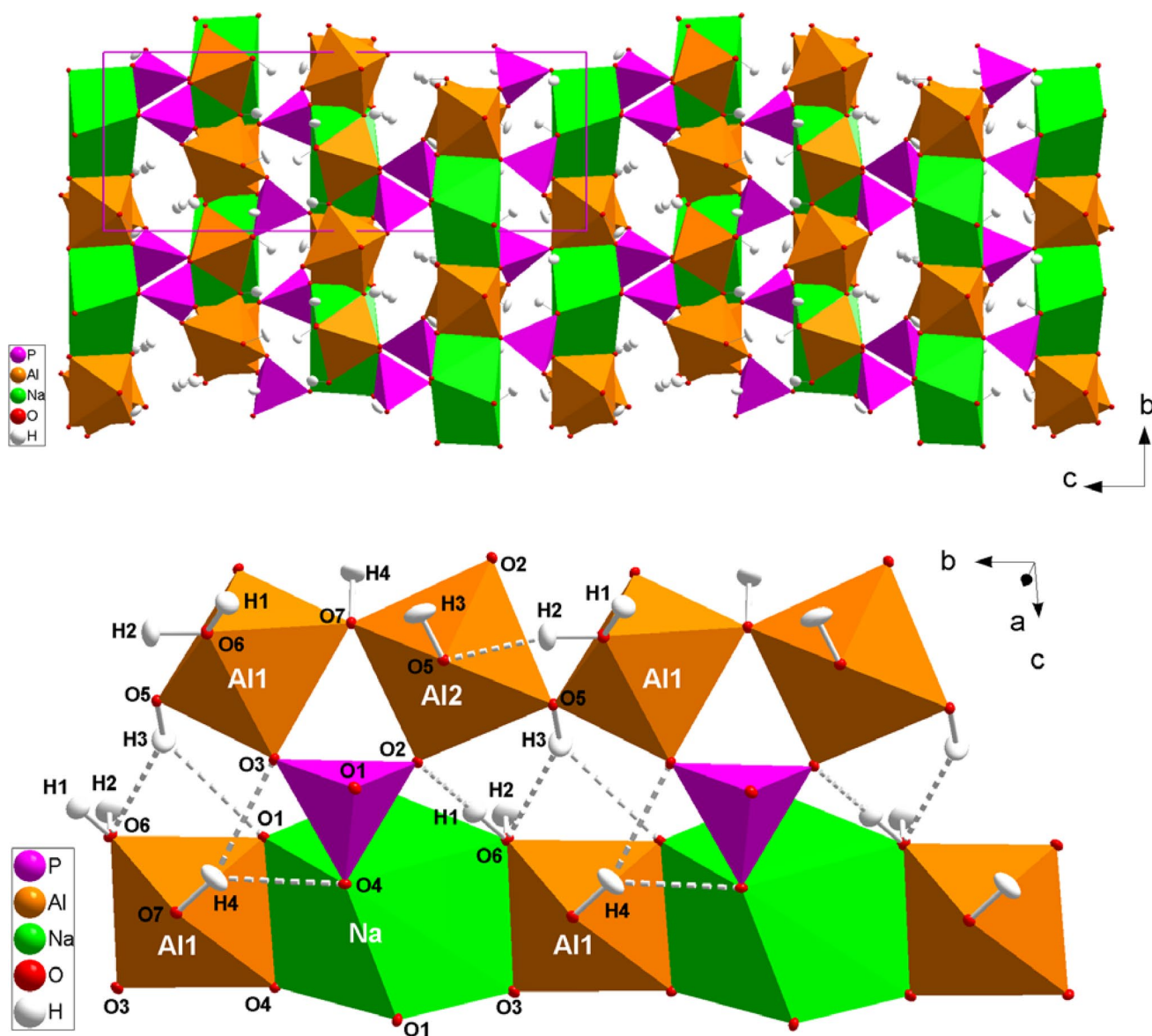


Fig. 1 Two views of the crystal structure of wardite based on the neutron structure refinement of this study (intensity data collected at 20 K). Displacement ellipsoid probability factor: 50%

the authors to locate the H sites, leaving open questions about configuration of the H_2O molecules and OH groups and, as a consequence, about the H-bonding scheme in the wardite structure. Wardite contains up to 18 wt% of H_2O ; therefore, the H content is not negligible. Based on electrostatic valences balance of the oxygen sites, Fanfani et al. (1970) suggested the potential occurrence of one independent H_2O -molecule and two independent hydroxyl-groups. A series of experiments on wardite have later been performed by infrared and Raman spectroscopies (e.g., Breitingner et al. 2004; Frost and Erickson 2005; Frost and Xi 2012). However, the full description of the active modes was hindered by the lack of a structure model in

which the H sites positions, their vibrational regimes and the H-bonding scheme were known.

More recently, Kampf et al. (2014) reported the occurrence of fluorowardite, ideally $\text{NaAl}_3(\text{PO}_4)_2(\text{OH})_2\text{F}_2 \cdot 2\text{H}_2\text{O}$. The structure was solved and described on the basis of a single-crystal X-ray structure refinement; a comparative description of the crystal structure of wardite and fluorowardite was provided.

In the framework of a long-term project on the crystal chemistry of hydrous phosphates (e.g., Gatta et al. 2013a, b, 2014a, b, 2015), we have reinvestigated the crystal structure and crystal chemistry of wardite by single-crystal neutron diffraction and electron microprobe analysis in

wavelength-dispersive mode (EPMA–WDS), to provide: (i) a reliable location of the proton sites and the real topological configuration of the OH groups and H₂O molecules, for a full description of the atomic relationship via the H bonds; (ii) the anisotropic displacement parameters of all the atomic sites, H sites included. To carry out this objective, single-crystal neutron diffraction data were collected at low temperature (20 K) to reduce the thermal displacement of the H sites.

Sample description and occurrence

The sample of wardite used in this study belongs to the collection of the Museum of Mineralogy of the University of Padova (catalogue number MM18662). The hand specimen is a group of pseudo-octahedral gem-quality crystals, formed by nearly equant tetragonal di-pyramids, striated perpendicular to [001], with pale blue-green colour and up to 1 cm in length. The larger crystals are transparent and vitreous. The specimen was collected at the Rapid Creek area, Canada. The Rapid Creek is a remote region in the north-eastern Yukon Territory, but it represents a remarkable deposit of uncommon and rare phosphate mineral species. Since the early 1970s, this area became, among mineralogists and mineral collectors, one of the most important sources for fine minerals such as arrojadite group minerals, augelite, collinsite, gorceixite, goyazite, kryzhanovskite, lazulite, wardite and whiteite (Robinson et al. 1992). This is also the type locality for several new iron-, magnesium-, manganese- and barium-phosphate minerals, including arrojadite-(KNa) (Moore et al. 1981), barićite (Sturman and Mandarino 1976), garyansellite (Sturman and Dunn 1984), gormanite (Sturman et al. 1981), kulanite (Mandarino and Sturman 1976), penikisite (Mandarino et al. 1977) and rapidcreekite (Roberts et al. 1986), a calcium, hydrate sulfate–carbonate.

Young and Roberston (1984) published a geological description of the Rapid Creek area, which is characterized by deposits of siderite and phosphatic ironstone embedded in shales and thick sequences of turbidite sandstones, named Blow River Formation, deposited during the early- to mid-Cretaceous. The phosphatic iron formation is composed of phosphate–siderite grains, detrital quartz and skeletal fragments in a matrix of sideritic mudstone. Most of the phosphate grains are not composed of apatite, but of rare phosphate minerals including arrojadite, gormanite and satterlyite. At Rapid Creek, well-crystallized phosphates occur within a set of rigid fracture which cross-cuts the Blow River Formation, where a typical fracture-filling mineral assemblage is related to the composition of the hosting rocks (Robertson 1982). Robertson (1982) identified four major mineral assemblages: (1) Ba-rich set of fractures cross-cutting conglomerates, (2) Ca-rich fractures cross-cutting

mudstones, (3) Fe–Mg–Mn rich set of fractures cross-cutting sandstones, and (4) Na-rich set of fractures cross-cutting phosphatic sandstones. The wardite sample used for this study is associated with spheroidal aggregates of millimetric greenish-bluish gormanite and rhombohedral brown vitreous millimetric crystals of siderite, probably related to the type 3 set of fractures as reported by Robertson (1982).

There is no geological evidence of the presence of an igneous activity in the area; the host rock is a sedimentary iron-rich formation. Fluid inclusion studies indicate that the sequence of crystallization of phosphates at Rapid Creek occurred between 180 and 200 °C, with quartz, lazulite and arrojadite, which represent the first minerals to crystallize, whilst wardite occurs as late stage phosphate. Except for minor illite and chlorite observed in the shales, no lawsonite, laumontite or pyrophyllite occur in the sedimentary rocks at Rapid Creek (Robertson 1982). For such a reason, the fracture-filling minerals were probably formed in the uppermost diagenesis to the lowermost range of regional metamorphism (Robinson et al. 1992).

Experimental methods

The chemical composition of the wardite used in this study was obtained using a CAMECA SX-50 electron microprobe equipped with four wavelength-dispersive spectrometers and one energy-dispersive spectrometer at the laboratory of microanalysis of the Institute for Geosciences and Earth Resources of CNR (Padova). The operating conditions were 20 kV accelerating voltage, 5 nA beam current and 10 µm beam diameter. Counting times were 10 s at the peak and 5 s at the background for major elements, and 20–100 s at peak and background for minor elements. X-ray counts were converted into oxide weight percentages using the PAP correction program (Pouchou and Pichoir 1991). Calibration was performed using natural and synthetic international standards, in part supplied by Cameca and in part kindly provided by the Smithsonian National Museum of Natural History (Smithsonian Microbeam Standards). The following reference materials, lines, and analyzing crystals were used: wollastonite (SiK α -TAP); diopside (CaK α -PET); albite (NaK α -TAP); fluorapatite (PK α -TAP); corundum (AlK α -TAP); MnTiO₃ (TiK α -PET); FeO (FeK α -LIF); MnTiO₃ (MnK α -LIF); orthoclase (KK α -PET); AsGa (AsL α , TAP). The elements K and As (and even F) were sought, but resulted below the experimental detection limits (i.e., less than 0.03 wt%). Minor evidence of sample dehydration, under the electron beam, was observed. Further details pertaining to the microprobe chemical analysis are given in Table 1.

Neutron diffraction data were collected on the four-circle diffractometer D19 at ILL (Grenoble, France)

Table 1 EPMA-WDS chemical analysis of wardite from Rapid Creek, Yukon, Canada. Average composition based on 14 point analysis

Oxides	Wt%	<i>e.s.d.</i>
Na ₂ O	7.02	6.29–7.43
Al ₂ O ₃	37.84	36.53–39.31
SiO ₂	0.03	0.01–0.06
P ₂ O ₅	37.28	36.65–37.80
CaO	0.12	0.07–0.17
TiO ₂	0.10	0.04–0.15
MnO	0.02	0.01–0.06
Fe ₂ O ₃	0.93	0.50–1.45
H ₂ O	16.85	
Total	100.19	
Elements	<i>a.p.f.u</i>	
Na	0.91	
Ca	0.01	
Al	2.97	
Fe ³⁺	0.05	
Ti	0.01	
Mn	0.00	
P	2.10	
H ⁺	7.48	

Analysis calculated on the basis of 14 anions

Fe₂O₃ calculated from FeO_{tot} obtained by microprobe analysis

Fixed (OH)_{Σ=4}

The empirical formula of wardite results:

(Na_{0.91}Ca_{0.01})_{Σ=0.92}(Al_{2.97}Fe³⁺_{0.05}Ti_{0.01})_{Σ=3.03}(P_{2.10}O₈)(OH)₄·1.74H₂O

with Cu(331)-monochromated radiation (take-off angle $2\theta_M = 70^\circ$), providing neutrons with a wavelength of 0.9460 Å. The sample was glued on a $\phi = 0.5$ mm vanadium pin and placed on a close-circuit displax device operated at 20.0(5) K (Archer and Lehmann 1986). The measurement strategy consists of omega (ω) scans of 64 or 79° with steps of 0.07° at different χ and φ positions. A total of 25 ω -scans were collected to complete almost a half-Ewald sphere. The Multi-Detector Acquisition Data Software (MAD) from ILL was used for data collection. The unit-cell determination was done by using PFIND and DIRAX programs (Duisenberg 1992). The integration of the raw data and refinement of the UB-matrix, including the off-sets, were done using RETREAT and RAFD19 programs, respectively (Wilkinson et al. 1988). The lattice was found to be metrically tetragonal, and the reflections conditions agreed with the space group $P4_12_12$, as previously reported by Fanfani et al. (1970). A total of 20,478 reflections were integrated, out of which 3109 were unique reflections (Laue group $4/mmm$, $R_{\text{int}} = 0.0411$). The absorption correction, mainly due to the hydrogen

Table 2 Details of neutron data collection and refinement of wardite

<i>T</i> (K)	20.0(5)
Crystal shape	Prism
Crystal volume (mm)	2×2×3
Crystal colour	Pale blue-green
Unit-cell parameters	$a = b = 7.0577(5)$ Å $c = 19.0559(5)$ Å
Chemical formula	NaAl ₃ (PO ₄) ₂ (OH) ₄ ·2H ₂ O
Space group	$P4_12_12$
<i>Z</i>	4
Radiation type	neutron
Wavelength (Å)	0.94602
Diffractionmeter	D19 four circle -ILL
Data collection method	ω -scan
Max. 2θ (°)	122.25
	$-12 \leq h \leq +12$
	$-12 \leq k \leq +7$
	$-34 \leq l \leq +35$
Measured reflections	20,478
Unique reflections	3109
Unique reflections with $F_o > 4\sigma(F_o)$	3106
Refined parameters	129
Extinction coeff.	0.0060(7)
R_{int}	0.0411
R_σ	0.0214
$R_1(F)$ with $F_o > 4\sigma(F_o)$	0.0219
$R_1(F)$ for all reflections	0.0221
$wR_2(F^2)$	0.0518
GooF	1.195
Residuals (fm/Å ³)	-0.68/+0.68

Statistical parameters according to the Shelxl-2014 definition (Sheldrick 2008, 2014)

content of the sample (ca. 0.132 mm⁻¹), was carried out using D19abs program (Matthewman et al. 1982). Further details pertaining to the data collection strategy are listed in Table 2 and in Gatta et al. (2018).

Anisotropic crystal structure refinement based on the neutron intensity data was done in the space group $P4_12_12$ using the SHELXL-2014 software (Sheldrick 2008, 2014), starting from the structure model of Fanfani et al. (1970), without any H atom. The neutron scattering lengths of Na, Al, Fe, P, O and H were taken from Sears (1986). Secondary isotropic extinction effect was corrected according to the formalism of Larson (1967), as implemented in the SHELXL package. Convergence was rapidly reached after the first cycles of refinement with a series of intense negative residual peaks in the final difference-Fourier map of the nuclear density (Fig. 2). Minima in the difference-Fourier maps of the nuclear density showed no evidence of positional or dynamic disorder (Fig. 2). Further cycles of refinement were done with H sites assigned to these peaks (as H

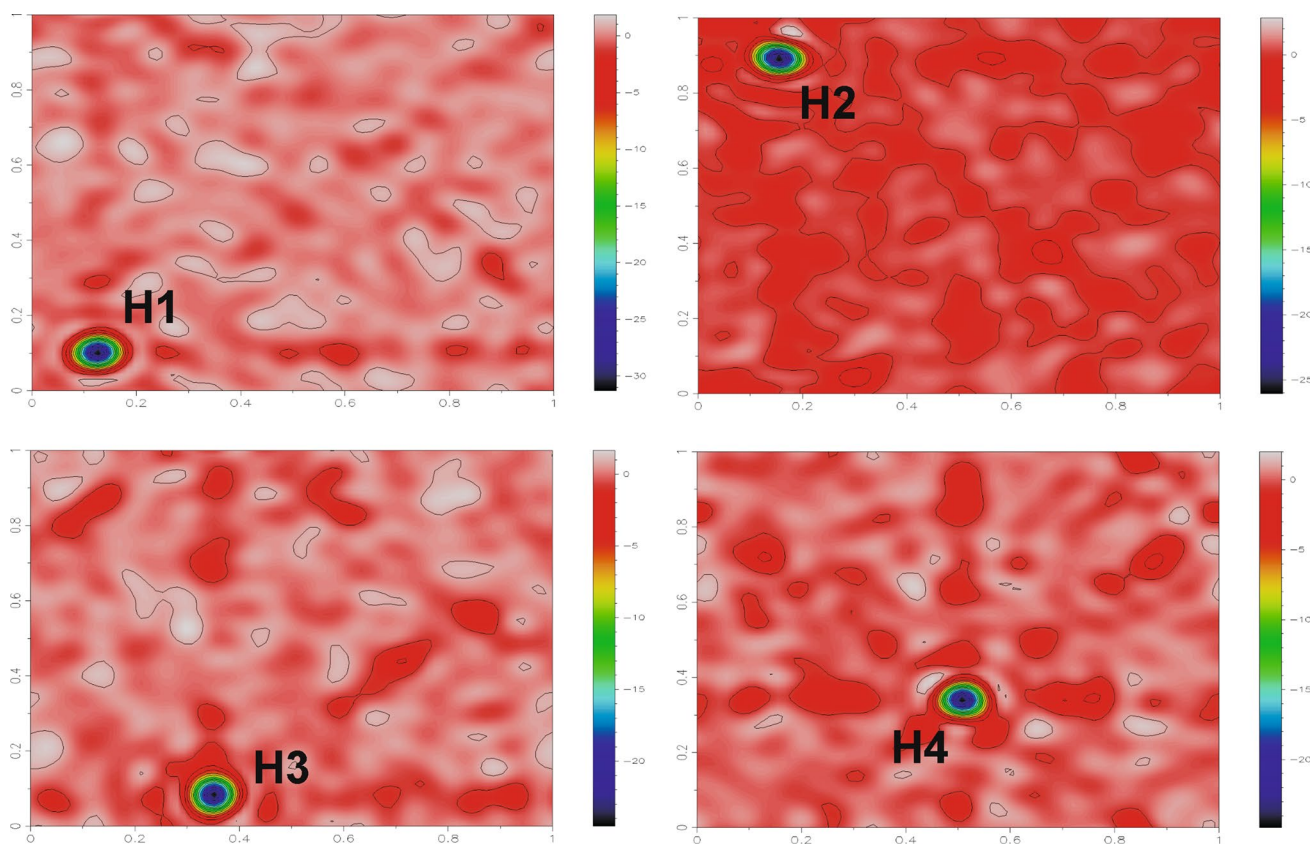


Fig. 2 Difference-Fourier maps of the nuclear density (xy sections, x horizontal; $z \sim 0.15$ for the H1 map, $z \sim 0.19$ for the H2 map, $z \sim -0.09$ for the H3 map, $z \sim 0.18$ for the H4 map) calculated with coefficients $F_o - F_c$ and phased by F_c . The F_c were calculated from a structural

model without the H sites. Minima, ascribable to the missing H sites (as H has negative neutron scattering length) are visible. Color bar unit: $\text{fm}/\text{\AA}^3$

has a negative neutron scattering length). At the end of the refinement (with $R_1(F) = 0.0219$ for 3106 reflections with $F_O > 4\sigma(F_O)$ and 129 refined parameters), all variable parameters converged with all the principal mean-square atomic displacement parameters positive, including those for the H sites. The variance–covariance matrix showed no significant correlation among the refined variables. Further details pertaining to the structure refinement strategy are given in Table 2. Coordinates of the atomic sites and displacement parameters are listed in Tables 3 and 4; selected interatomic distances and angles are given in Table 5.

Results and discussion

The EPMA–WDS analysis of the wardite sample used in this study confirms the general findings previously reported in the literature: the ideal formula of this mineral is $\text{NaAl}_3(\text{PO}_4)_2(\text{OH})_4 \cdot 2\text{H}_2\text{O}$; Na is replaced by a very modest fraction of Ca; P (in tetrahedral coordination) is replaced by a low fraction of Si; Al (in octahedral configuration) is replaced by Fe, Mn and Ti (Table 1).

Table 3 Refined fractional atomic coordinates and equivalent/isotropic displacement factors (\AA^2), based on the neutron structure refinement

Site	x/a	y/b	z/c	U_{eq}
P	0.14076(7)	0.36564(7)	0.34911(2)	0.00306(7)
Al1	0.39588(11)	0.10694(11)	0.25770(4)	0.0029(1)
Al2	0.10298(11)	0.10298(11)	0	0.0031(1)
Na	0.37371(11)	0.37371(11)	0.5	0.0063(1)
O1	-0.03785(7)	0.42506(7)	0.30966(3)	0.00483(7)
O2	0.29995(7)	0.51346(7)	0.33752(2)	0.00443(7)
O3	0.20513(7)	0.17351(7)	0.32071(3)	0.00497(7)
O4	0.09981(7)	0.35105(7)	0.42774(2)	0.00469(7)
O5	0.13341(7)	0.35260(7)	-0.03932(2)	0.00453(7)
O6	0.18718(7)	0.03209(7)	0.19138(3)	0.00585(7)
O7	0.40821(7)	0.34989(7)	0.21653(2)	0.00480(7)
H1	0.1264(2)	0.1027(2)	0.15197(6)	0.0178(2)
H2	0.1584(2)	-0.1030(2)	0.18760(7)	0.0199(2)
H3	0.0827(2)	0.3519(2)	-0.0860(1)	0.0232(2)
H4	0.5094(2)	0.3408(2)	0.18255(7)	0.0215(2)

U_{eq} is defined as one-third of the trace of the orthogonalised U_{ij} tensor. All the sites show s.o.fs of 100%

Table 4 Refined displacement parameters (\AA^2) in the expression: $-2\pi^2[(ha^*)^2U_{11} + \dots + 2hka^*b^*U_{12} + \dots + 2klb^*c^*U_{23}]$ and root-mean-square displacement amplitude (RMS, \AA), based on the neutron structure refinement of wardite

	U_{11}	U_{22}	U_{33}	U_{12}	U_{13}	U_{23}
P	0.0030(2)	0.0030(2)	0.0032(1)	0.0001(1)	-0.0001(1)	-0.0002(1)
Al1	0.0030(2)	0.0028(2)	0.0031(2)	0.0001(2)	0.0000(2)	0.0002(2)
Al2	0.0027(2)	0.0027(2)	0.0037(3)	-0.0002(2)	0.0002(2)	-0.0002(2)
Na	0.0062(2)	0.0062(2)	0.0067(3)	0.0001(3)	0.0000(2)	0.0000(2)
O1	0.0038(1)	0.0055(2)	0.0052(1)	0.0003(1)	-0.0008(1)	0.0012(1)
O2	0.0044(2)	0.0044(2)	0.0046(1)	-0.0012(1)	0.0001(1)	-0.0001(1)
O3	0.0054(2)	0.0038(2)	0.0058(2)	0.0004(1)	0.0010(1)	-0.0008(1)
O4	0.0046(1)	0.0058(2)	0.0037(1)	0.0003(1)	0.0003(1)	0.0002(1)
O5	0.0052(1)	0.0037(1)	0.0047(1)	0.0001(1)	-0.0003(1)	0.0001(1)
O6	0.0063(2)	0.0055(2)	0.0058(1)	-0.0003(1)	-0.0014(1)	0.0003(1)
O7	0.0051(1)	0.0038(1)	0.0055(1)	0.0001(1)	0.0007(1)	-0.0001(1)
H1	0.0201(4)	0.0182(4)	0.0151(3)	0.0020(3)	-0.0030(3)	0.0033(3)
H2	0.0241(5)	0.0119(3)	0.0236(5)	-0.0036(3)	-0.0035(4)	-0.0004(3)
H3	0.0365(7)	0.0197(5)	0.0133(4)	0.0020(5)	-0.0106(4)	-0.0014(3)
H4	0.0225(5)	0.0193(5)	0.0227(5)	0.0015(4)	0.0128(4)	0.0009(4)
	RMS-min	RMS-mid	RMS-max	max/min		
P	0.05405	0.05430	0.05762	1.066		
Al1	0.05175	0.05428	0.05644	1.091		
Al2	0.05029	0.05230	0.06180	1.229		
Na	0.07756	0.07937	0.08188	1.056		
O1	0.05591	0.06932	0.08093	1.448		
O2	0.05612	0.06734	0.07493	1.335		
O3	0.05677	0.07116	0.08144	1.435		
O4	0.05978	0.06772	0.07694	1.287		
O5	0.06112	0.06750	0.07285	1.192		
O6	0.06802	0.07356	0.08673	1.275		
O7	0.06180	0.06797	0.07727	1.250		
H1	0.10714	0.14260	0.14685	1.371		
H2	0.10362	0.14534	0.16661	1.608		
H3	0.09549	0.13966	0.20222	2.118		
H4	0.09881	0.13837	0.18875	1.910		

Previous experimental findings confirmed that iron occurs as Fe^{3+} in wardite (Vassilikou-Dova 1993). The empirical formula of wardite used in this study is: $(\text{Na}_{0.91}\text{Ca}_{0.01})_{\Sigma=0.92}(\text{Al}_{2.97}\text{Fe}^{3+}_{0.05}\text{Ti}_{0.01})_{\Sigma=3.03}(\text{P}_{2.10}\text{O}_8)(\text{OH})_4 \cdot 1.74\text{H}_2\text{O}$ (Table 1).

The neutron structure refinement of this study, based on intensity data collected at 20 K, is consistent with the general structural model previously obtained by Fanfani et al. (1970), based on single-crystal X-ray intensity data collected at room conditions: wardite structure consists of sheets made by edge-sharing Na-polyhedra (with coordination number = 8) and Al-octahedra along with vertex-sharing Al-octahedra, parallel to (001), connected by P-tetrahedra and H bonds to form a (001) layer-type structure, which well explains the pronounced {001} cleavage of the wardite crystals (Fig. 1; Table 5).

Accordingly, strong structural homologies occur between the crystal structure of wardite and fluorowardite (ideally $\text{NaAl}_3(\text{PO}_4)_2(\text{OH})_2\text{F}_2 \cdot 2\text{H}_2\text{O}$, Kampf et al. 2014). Our data show that in wardite, the P-tetrahedron is almost regular (with $\Delta(\text{P}-\text{O})_{\text{max}} \sim 0.02 \text{ \AA}$, i.e., the difference between the longest and the shortest bond distances), whereas the two independent Al-octahedra are slightly distorted ($\Delta(\text{Al1}-\text{O})_{\text{max}} \sim 0.15 \text{ \AA}$, $\Delta(\text{Al2}-\text{O})_{\text{max}} \sim 0.03 \text{ \AA}$). Four crystallographically independent H sites occur into the structure of wardite (namely, H1–H4, Table 3). In particular:

- H1 and H2 form a H_2O molecule with the O6 site (oxygen site shared by adjacent Na-polyhedron and Al-octahedron, Fig. 1), with $\text{H1}-\text{O6}-\text{H2} = 110.0(1)^\circ$, $\text{O6}-$

Table 5 Relevant bond distances (Å) and angles (°) based on the neutron structure refinement

P–O1	1.5265(7)	O1–P–O2	110.10(4)	O5–H3	0.959(1)
P–O2	1.5490(7)	O1–P–O3	108.34(4)	O5–H3*	0.986
P–O3	1.5291(7)	O1–P–O4	110.18(4)	O5–H3···O1	139.9(1)
P–O4	1.5295(5)	O2–P–O3	109.35(4)	O5···O1	3.347(1)
		O2–P–O4	108.79(4)	H3···O1	2.556(1)
Al1–O1	1.8661(9)	O3–P–O4	110.07(4)	O5–H3···O6	148.5(1)
Al1–O3	1.8641(9)			O5···O6	3.205(1)
Al1–O4	1.9165(9)	O1–Al1–O3	176.37(5)	H3···O6	2.347(1)
Al1–O5	1.9047(9)	O1–Al1–O4	88.48(4)		
Al1–O6	2.0114(9)	O1–Al1–O5	92.57(4)	O6–H1	0.998(1)
Al1–O7	1.8876(9)	O1–Al1–O6	89.72(4)	O6–H1*	1.013
		O1–Al1–O7	85.43(4)	O6–H1···O2	174.4(1)
Al2–O2 × 2	1.9105(6)	O3–Al1–O4	95.16(4)	O6···O2	2.613(1)
Al2–O5 × 2	1.9265(9)	O3–Al1–O5	87.44(4)	H1···O2	1.617(1)
Al2–O7 × 2	1.8983(9)	O3–Al1–O6	86.68(4)		
		O3–Al1–O7	94.13(4)	O6–H2	0.978(1)
Na–O4 × 2	2.3788(8)	O4–Al1–O5	91.39(4)	O6–H2*	0.996
Na–O1 × 2	2.4756(7)	O4–Al1–O6	173.67(4)	O6–H2···O5	160.1(1)
Na–O6 × 2	2.5659(10)	O4–Al1–O7	95.26(4)	O6···O5	2.852(1)
Na–O3 × 2	2.7199(8)	O5–Al1–O6	82.63(4)	H2···O5	1.913(1)
		O5–Al1–O7	173.00(5)	H1–O6–H2	110.0(1)
		O6–Al1–O7	90.64(4)		
				O7–H4	0.966(1)
		O2–Al2–O2	177.74(5)	O7–H4*	0.989
		O2–Al2–O5	92.78(4)	O7–H4···O3	160.5(1)
		O2–Al2–O5	85.58(3)	O7···O3	3.373(1)
		O2–Al2–O7	89.83(4)	H4···O3	2.447(1)
		O2–Al2–O7	91.74(3)	O7–H4···O4	137.9(1)
		O5–Al2–O5	86.98(4)	O7···O4	3.231(1)
		O5–Al2–O7	90.70(3)	H4···O4	2.449(1)
		O5–Al2–O7	174.75(4)		
		O7–Al2–O7	91.98(4)		

*Bond distance corrected for “riding motion” following Busing and Levy (1964)

H1* = 1.013 Å and O6–H2* = 0.996 Å (* corrected for “riding motion” effect, Table 5).

- H3 forms a hydroxyl group with the O5 site (as bridging oxygen site shared by adjacent Al-octahedra, Fig. 1), with O5–H3* = 0.986 Å (Table 5).
- H4 forms a hydroxyl group with the O7 site (as bridging oxygen site shared by adjacent Al-octahedra, Fig. 1), with O7–H4* = 0.989 Å (Table 5).

The H-bonding scheme in the structure of wardite is now well defined:

- The H1 site is H-bonded to the O2 site, with O6–H1···O2 = 174.4(1)° and H1···O2 = 1.617(1) Å (Fig. 1; Table 5).

- The H2 site is H-bonded to the O5 site, with O6–H2···O5 = 160.1(1)° and H2···O5 = 1.913(1) Å (Fig. 1; Table 5).
- The H3 site shows a bifurcated bonding scheme with O5–H3···O1 = 139.9(1)° and H3···O1 = 2.556(1) Å, and O5–H3···O6 = 148.5(1)° and H3···O6 = 2.347(1) Å (Fig. 1; Table 5).
- The H4 site also shows a bifurcated bonding scheme with O7–H4···O3 = 160.5(1)° and H4···O3 = 2.447(1) Å, and O7–H4···O4 = 137.9(1)° and H4···O4 = 2.449(1) Å (Fig. 1; Table 5).

Whereas the H1–O6–H2 molecule experiences two strong H bonds, as corroborated by the bonding geometry, the two hydroxyl groups show relatively weak interactions

(Table 5). The H1–O6–H2 angle (Table 5) is still in the range of the observed H–O–H angles in solid-state materials (Chiari and Ferraris 1982; Steiner 1998 and references therein; Gatta et al. 2008, 2012, 2019; Lotti et al. 2017). The hydrogen bonds of the H₂O molecule show O–H···O angles $\geq 160^\circ$ (Table 5), with a configuration energetically favorable (i.e., approaching linearity, Steiner 1998); the bifurcated H-bonding configuration of the two independent hydroxyl groups leads to a bonding geometry energetically more costly. In fluorowardite, one of the two independent hydroxyl groups is replaced by fluorine, but the H₂O content is virtually identical to that of wardite: the replacement OH[−] → F[−] is possible, without any significant rearrangement of the structure, because of the (very) weak H bonds generated by the hydroxyl group. The H-bonding scheme in the structure of wardite here described is compatible with the findings based on vibrational spectroscopies (e.g., Breiteringer et al. 2004; Frost and Erickson 2005; Frost and Xi 2012). A more robust description of the active IR vibrational modes, dictated by the H bonds, can now be delivered on the basis of the experimental findings of this study.

As shown by the root-mean-square components of the displacement ellipsoids, oxygen and hydrogen atoms have slightly larger anisotropic displacement parameters compared to the other sites (populated by P, Al and Na). The maximum ratio of the *max* and *min* root-mean-square components of the displacement ellipsoids is observed for the protons of the hydroxyl groups (i.e., O5–H3 and O7–H4, Table 4), which experience bifurcated H-bonding schemes.

The neutron structure refinement does not show evidence of partial site occupancy of the H₂O group (Table 3). In this light, the molecular H₂O fraction of the calculated unit formula (i.e., 1.74 molecules p.f.u., Table 1), in which the H₂O wt% was assumed considering (OH)_{Σ=4}, is likely underestimated: according to the neutron structure refinement, wardite contains 2.0 molecules p.f.u.. The underestimation of the (total) water content could be related with the replacement of the OH group by fluorine, as observed in fluorowardite, and neither X-ray nor neutron diffraction is able to distinguish unambiguously between O and F as their scattering factors/lengths are quite similar. The EPMA–WDS analysis of the wardite used in this study does not show a significant content of fluorine; however, evidence of dehydration under the electron beam were observed during the EPMA–WDS analysis.

Acknowledgements The authors thank the Institut Laue-Langevin (Grenoble, France), for the allocation of the beamtime and the Institute for Geosciences and Earth Resources of CNR (Padova) for the microprobe analysis of wardite. Two anonymous reviewers and the Editor, M. Rieder, are thanked. This manuscript is dedicated to Pier Francesco Zanazzi (b. 1939), professor of Mineralogy and Crystallography at the University of Perugia (Italy), who solved and refined the structure of

wardite with Luca Fanfani and Antonio Nunzi in 1970, on the occasion of his 80th birthday.

References

- Archer J, Lehmann MS (1986) A simple adjustable mount for a two-stage cryorefrigerator on an Eulerian cradle. *J Appl Crystallogr* 19:456–459
- Breiteringer DK, Belz HH, Hajba L, Komlosi V, Mink J, Brehm G, Colognesi D, Parker SF, Schwab RG (2004) Combined vibrational spectra of natural wardite. *J Mol Struct* 706:95–99
- Busing WR, Levy HA (1964) The effect of thermal motion on the estimation of bond lengths from diffraction measurements. *Acta Crystallogr* 17:142–146
- Chiari G, Ferraris G (1982) The water molecules in crystalline hydrates studied by neutron diffraction. *Acta Crystallogr B* 38:2331–2341
- Davison JM (1896) Wardite: a new hydrous basic phosphate of alumina. *Am J Sci* 2:154–155
- Duisenberg AJM (1992) Indexing in single-crystal diffractometry with an obstinate list of reflections. *J Appl Crystallogr* 25:92–96
- Fanfani L, Nunzi A, Zanazzi PF (1970) The crystal structure of wardite. *Mineral Mag* 37:598–605
- Frost RL, Erickson KL (2005) Near-infrared spectroscopic study of selected hydrated hydroxylated phosphates. *Spectrochim Acta A* 61:45–50
- Frost RL, Xi YA (2012) Vibrational spectroscopic study of the phosphate mineral Wardite NaAl₃(PO₄)₂(OH)₄·2H₂O. *Spectrochim Acta A* 93:155–163
- Gatta GD, Rotiroti N, McIntyre GJ, Guastoni A, Nestola F (2008) New insights into the crystal chemistry of epididymite and eudidymite from Malosa, Malawi: a single-crystal neutron diffraction study. *Am Mineral* 93:1158–1165
- Gatta GD, McIntyre GJ, Swanson GJ, Jacobsen SD (2012) Minerals in cement chemistry: a single-crystal neutron diffraction and Raman spectroscopic study of thaumasite, Ca₃Si(OH)₆(CO₃)(SO₄)·12H₂O. *Am Mineral* 97:1060–1069
- Gatta GD, Vignola P, Meven M, Rinaldi R (2013a) Neutron diffraction in gemology: single-crystal diffraction study of brazilianite, NaAl₃(PO₄)₂(OH)₄. *Am Mineral* 98:1624–1630
- Gatta GD, Nénert G, Vignola P (2013b) Coexisting hydroxyl groups and H₂O molecules in minerals: a single-crystal neutron diffraction study of eosphorite, MnAlPO₄(OH)₂·H₂O. *Am Mineral* 98:1297–1301
- Gatta GD, Jacobsen SD, Vignola P, McIntyre GJ, Guastella G, Abate LF (2014a) Single-crystal neutron diffraction and Raman spectroscopic study of hydroxylherderite, CaBePO₄(OH,F). *Mineral Mag* 78:723–737
- Gatta GD, Vignola P, Meven M (2014b) On the complex H-bonding network in paravauxite, Fe²⁺Al₂(PO₄)₂(OH)₂·8H₂O: a single-crystal neutron diffraction study. *Mineral Mag* 78:841–850
- Gatta GD, Redhammer GJ, Vignola P, Meven M, McIntyre GJ (2015) Single-crystal neutron diffraction and Mössbauer spectroscopic study of hureaulite, (Mn,Fe)₅(PO₄)₂(HPO₄)₂(H₂O)₄. *Eur J Mineral* 28:93–103
- Gatta GD, Fabelo Rosa OR, Fernandez-Diaz MT (2018) On the crystal chemistry of the wardite, NaAl₃(PO₄)₂(OH)₄ × 2H₂O. Institut Laue-Langevin (ILL, Grenoble). <https://doi.org/10.52911/ILL-DATA.5-11-430>
- Gatta GD, Hälenius U, Bosi F, Cañadillas-Delgado L, Fernandez-Diaz MT (2019) Minerals in cement chemistry: a single-crystal neutron

- diffraction study of ettringite, $\text{Ca}_6\text{Al}_2(\text{SO}_4)_3(\text{OH})_{12} \cdot 27\text{H}_2\text{O}$. *Am Mineral*. <https://doi.org/10.2138/am-2019-6783> (in press)
- Heritsch H (1955) Die Raumgruppe von Wardit. *Tschemm's Min Petr Mitt* 5:246–251
- Hurlbut CS (1952) Wardite from beryl mountain, New Hampshire. *Am Mineral* 37:849–852
- Kampf AR, Adams PM, Housley RM, Rossman GR (2014) Fluorowardite, $\text{NaAl}_3(\text{PO}_4)_2(\text{OH})_2\text{F}_2 \cdot 2\text{H}_2\text{O}$, the fluorine analogue of wardite from the Silver Coin mine, Valmy, Nevada. *Am Mineral* 99:804–810
- Larson AC (1967) Inclusion of secondary extinction in least-squares calculations. *Acta Crystallogr* 23:664–665
- Lotti P, Gatta GD, Demitri N, Guastella G, Rizzato S, Ortenzi MA, Magrini F, Comboni D, Guastoni A, Fernandez-Diaz MT (2017) Crystal-chemistry and temperature behavior of the natural hydrous borate colemanite, a mineral commodity of boron. *Phys Chem Minerals* 45:405–422
- Mandarino JA, Sturman BD (1976) Kulanite, a new barium iron aluminum phosphate from the Yukon Territory, Canada. *Can Mineral* 14:127–131
- Mandarino JA, Sturman BD, Corlett MI (1977) Penikisite, the magnesium analogue of kulanite, from the Yukon Territory, Canada. *Can Mineral* 15:393–395
- Matthewman JC, Thompson P, Brown PJ (1982) The Cambridge crystallography subroutine library. *J Appl Crystallogr* 15:167–171
- Moore PB, Araki T, Merlino S, Mellini M, Zanazzi PF (1981) The arjadite-dickinsonite series, $\text{KNa}_4\text{Ca}(\text{Fe}, \text{Mn})_{14}^{2+}\text{Al}(\text{OH})_2(\text{PO}_4)_{12}$: crystal structure and crystal chemistry. *Am Mineral* 66:1034–1049
- Pouchou J-L, Pichoir F (1991) Quantitative analysis of homogeneous or stratified microvolumes applying the method “PAP”. In: Heinrich KFJ, Newbury DE (eds) *Electron probe quantitation*. Plenum Press, New York, pp 31–75
- Roberts AC, Ansell HG, Jonasson IR, Grice JD, Ramik RA (1986) Rapidcreekite, a new hydrated calcium sulfate-carbonate from the Rapid Creek area, Yukon Territory. *Can Mineral* 24:51–54
- Robertson BT (1982) Occurrence of epigenetic phosphate minerals in a phosphatic iron formation, Yukon Territory. *Can Mineral* 20:177–187
- Robinson GW, Van Velthuisen J, Ansell HG, Sturman BD (1992) Mineralogy of the Rapid Creek and Big Fish river area, Yukon Territory. *Mineral Rec* 23:1–47
- Sears VF (1986) Neutron scattering lengths and cross-sections. In: Sköld K, Price DL (eds) *Neutron scattering, methods of experimental physics*, vol 23A. Academic Press, New York, pp 521–550
- Sheldrick GM (2008) A short history of SHELX. *Acta Crystallogr* A64:112–122
- Sheldrick GM (2014) SHELXL-2014. Programs for crystal structure determination and refinement. University of Göttingen, Germany
- Steiner T (1998) Opening and narrowing of the water H–O–H angle by hydrogen-bonding effects: re-inspection of neutron diffraction data. *Acta Crystallogr B* 54:464–470
- Sturman BD, Dunn PJ (1984) Garyansellite, a new mineral from Yukon Territory. *Am Mineral* 69:207–209
- Sturman BD, Mandarino JA (1976) Baričite, the magnesium analogue of vivianite, from the Yukon Territory, Canada. *Can Mineral* 14:403–406
- Sturman BD, Mandarino JA, Mrose ME, Dunn PJ (1981) Gormanite, $\text{Fe}_3^{2+}\text{Al}_4(\text{PO}_4)_4(\text{OH})_6 \cdot 2\text{H}_2\text{O}$, the ferrous analogue of souzalite, and new data for souzalite. *Can Mineral* 19:381–387
- Vassilikou-Dova AB (1993) An EPR study of trivalent iron in wardite. *Appl Magn Reson* 5:25–29
- Wilkinson C, Khamis HW, Stansfield RFD, McIntyre GJ (1988) Integration of single-crystal reflections using area multidetectors. *J Appl Crystallogr* 21:471–478
- Young FG, Robertson BT (1984) The Rapid Creek formation: an Albian Flysch-related phosphatic iron formation in Northern Yukon Territory. In: Stott DF, Glass DJ (eds) *The mesozoic of Middle North America*. Canadian Society of Petroleum Geologists Memoir 9, Calgary, pp 361–372